Surface Science 299/300 (1994) 219–232
North-Holland

surface science

Low energy ion scattering and recoiling

J. Wayne Rabalais
Department of Chemistry, University of Houston, Houston, TX 77204-5641, USA

Received 24 January 1993; accepted for publication 2 April 1993

Ion scattering spectrometry was developed as a surface elemental analysis technique in the late 1960's. Further developments during the 1970's and 80's revealed the ability to obtain surface structural information. The recent use of time-of-flight (TOF) methods has led to a surface crystallography that is sensitive to all elements, including hydrogen, and the ability to directly detect hydrogen adsorption sites. TOF detection of both neutrals and ions provides the high sensitivity necessary for non-destructive analysis. Detection of atoms scattered and recoiled from surfaces in simple collision sequences, together with calculations of shadowing and blocking cones, can now be used to make direct measurements of interatomic spacings and adsorption sites within an accuracy of $\lesssim 0.1$ Å. Structures are determined by monitoring the angular anisotropies in the scattered primary and recoiled target atom flux. Applications of such surface structure and adsorption site determinations are in the fields of catalysis, thin film growth, and interfaces. This article provides a short historical account of these developments along with some examples of the most recent capabilities of the technique.

1. Historical perspective

The origin of scattering experiments has its roots in the development of modern atomic theory at the beginning of this century. As a result of both the Rutherford experiment on the scattering of alpha particles (He nuclei) by thin metallic foils and the Bohr theory of atomic structure, a consistent model of the atom as a small massive nucleus surrounded by a large swarm of light electrons was confirmed. Following these developments, it was realized that the inverse process, namely analysis of the scattering pattern of ions from crystals, could provide information on composition and structure. This analysis is straightforward because the kinematics of energetic atomic collisions is accurately described by classical mechanics. Such scattering occurs as a result of the mutual Coulomb repulsion between the colliding atomic cores, that is the nucleus plus core electrons. The scattered primary atom loses some of its energy to the target atom. The latter, in turn, recoils into a forward direction. The final energies of the scattered and recoiled atoms and the directions of their trajectories are determined by the masses of the pair of atoms involved and the closeness of the collision. By analysis of these final energies and angular distributions of the scattered and recoiled atoms, the elemental composition and structure of the surface can be deciphered.

Low energy (1–10 keV) ion scattering spectrometry (ISS) had its beginning as a modern surface analysis technique with the 1967 work of Smith [1], which demonstrated both surface elemental and structural analysis for CO chemisorbed on Mo; screening of the scattering from C by the presence of O showed that CO chemisorbed on Mo with the C end down and the O end up. During the 1970's, work by Heiland and Taglauer [2], Brongersma et al. [3], Boers et al. [4], and Bronckers et al. [5] clearly demonstrated that direct structural information could be obtained from ISS.

Interest in ISS as a technique for investigating surface structure grew quickly after the 1982 work

SSDI 0039-6028(93)E0301-A

of Aono et al. [6], which showed that the use of backscattering angles near 180° greatly simplified the scattering geometry and interpretation. This allowed experimental determination of the shadow cone radii which could be applied to surfaces with unknown or reconstructed structures in order to determine surface geometry. There are two problems with this technique: (i) It analyzes only the scattered ions; these are typically only a very small fraction ($< 5\%$) of the total scattered flux. Thus, high primary ion doses are required for spectral acquisition which are potentially damaging to the surface and adsorbate structures. (ii) Neutralization probabilities are a function of the ion beam incidence angle α with the surface and the azimuthal angle δ along which the ion beam is directed. This is not a simple behavior since the probabilities depend on the distances of the ion to specific atoms. As a result, it is difficult to separate scattering intensity changes due to neutralization effects from those due to structural effects. Aono and Souda [7] also proposed the use of ion scattering to probe the spatial distributions of surface electrons. This work successfully demonstrated that the phenomenon of ion neutralization could be used to probe the electron orbital angular distributions, however, ambiguity remained due to the fact that the information was derived from analysis of the scattered ions only. It was difficult to separate ion neutralization effects from shadowing and blocking effects. In 1984 Niehus [8] proposed the use of alkali primary ions which have low neutralization probabilities, leading to higher scattering intensities and pronounced focusing effects. The contamination of the sample surface by the reactive alkali ions is a potential problem with this method. Buck and coworkers [9], who had been developing time-of-flight (TOF) methods for ion scattering since the mid 1970's, used TOF methods for surface structure analysis in 1984 and demonstrated the capabilities and high sensitivity of the technique when both neutrals and ions are detected simultaneously. In 1987 van Zoest et al. [10] demonstrated that TOF analysis of both the scattered and recoiled neutrals and ions provided much more information about surface structure, however, they did not have adequate resolution in the TOF mode to separate the scattered and recoiled particles; this limited the use of the recoil data.

Having been developing TOF methods for scattering and recoiling, spectral interpretation, and surface elemental analysis in our own laboratory since the early 1980's [11], our research group began to concentrate its efforts on surface structural determinations in the late 1980's. In 1989 [12] we published structural determinations for O and H on W{211} using TOF detection of scattered and recoiled neutrals plus ions with sufficient resolution to clearly separate the recoiled and scattered particles. The first TOF spectrometer system with long flight path for separation of the scattered and recoiled particles and continuous variation of the scattering θ and recoiling ϕ angles was developed in our laboratory and published in 1990 [13]. This coupling of TOF methods with detection of both scattered and recoiled particles has led to the development of time-of-flight scattering and recoiling spectrometry (TOF-SARS) as a tool for structural analysis [14].

Several research groups [15–35] throughout the world are now engaged in surface structure determinations using some form of keV ISS. The number of research papers concerning surface structure determinations by means of some form of low energy (< 10 keV) ion scattering and recoiling spectrometry published since 1975 are shown graphically in Fig. 1. It is obvious that the level of

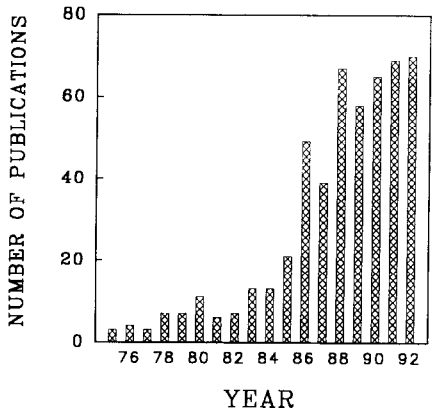

Fig. 1. Number of research papers concerned with surface structure determinations using some form of low energy (< 10 keV) ion scattering or recoiling published in recent years.

research activity in this field grew tremendously during the late 1980's.

This historical overview will concentrate on time-of-flight scattering and recoiling spectrometry (TOF-SARS) [14], for it is felt that this is the technique that will be most important in future applications. Also in this overview, emphasis will be placed on surface structure determinations rather than surface elemental analysis, for it is felt that TOF-SARS is capable of making unique contributions in the area of structure determination.

2. Basic physics underlying keV ion scattering and recoiling

There are two basic physical phenomena which govern atomic collisions in the keV range. First, repulsive interatomic interactions, described by the laws of classical mechanics, control the scattering and recoiling trajectories. Second, electronic transition probabilities, described by the laws of quantum mechanics, control the ion–surface charge exchange process.

2.1. Atomic collisions in the keV range

The dynamics of keV atomic collisions are well described as binary collisions between the incident ion and surface atoms [36]. When an energetic ion makes a direct collision with a surface atom, the surface atom is recoiled into a forward direction as shown in Fig. 2. Both the scattered and recoiled atoms have high, discrete kinetic energy distributions. According to the laws of conservation of energy and momentum, the energy E_S of an incident ion of mass M_1 and energy E_0 which is scattered from a target atom of mass M_2 into an angle θ is given by

$$E_S = E_0\left[\cos\theta + (A^2 \pm \sin^2\theta)^{1/2}/(1+A)\right]^2, \quad (1)$$

where $A = M_2/M_1$. For cases where $M_1 > M_2$, there exists a critical angle $\theta_c = \sin^{-1} A$ above which only multiple scattering can occur. Recoils that are ejected from single collisions of the projectile into an angle ϕ, that is direct recoils, have an energy E_R given by

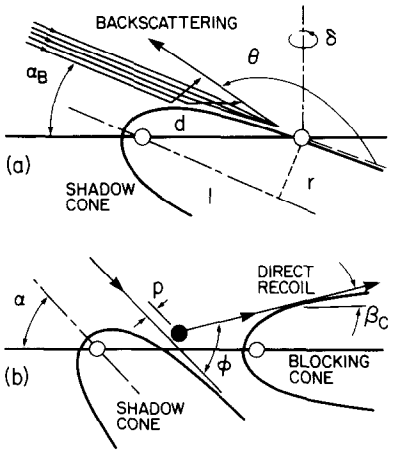

Fig. 2. Schematic illustrations of backscattering and shadowing and direct recoiling with shadowing and blocking.

$$E_R = E_0\left[4A/(1+A)^2\right]\cos^2\phi. \quad (2)$$

As a result of the energetic nature of the collisions, only atomic species are observed as direct recoils and their energies are independent of the chemical bonding environment.

2.2. Interatomic potentials

Although scattering in the keV range is dominated by repulsive potentials, it is not simply a hard sphere or billard ball collision where there is a clean "hit" or "miss". The partial penetration of the ion into the target atom's electron cloud results in bent trajectories even when there is not a "head-on" collision. This type of interaction is well described by a screened Coulomb potential [36] such as

$$V(r) = \left[Z_1 Z_2 e^2/R\right]\Phi(R/CR_s), \quad (3)$$

where R is the internuclear separation and the Z_i are the atomic numbers of the collision partners. Φ is a screening function which is determined by R, the screening radius R_s, and a scaling parameter C; there are several good approximations for Φ [36]. Using such a potential, one can determine the relationship between the scattering angle θ and the impact parameter p. The p is defined as

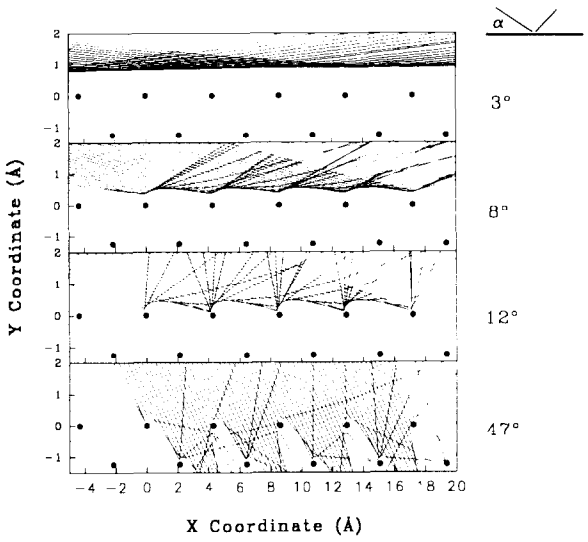

Fig. 3. Classical scattering trajectories for 4 keV Ne^+ impinging on a Ni surface at different incident angles α.

the minimum perpendicular distance from the target atom to the ion trajectory. A small value of p corresponds to a near head-on collision and backscattering and a large value corresponds to a glancing collision and forwardscattering. Similarly, the recoiling angle ϕ is also determined by p.

2.3. Shadowing and blocking cones

Considering a large number of ions with parallel trajectories impinging on a target atom, the ion trajectories are bent by the repulsive potential such that there is an excluded volume, called the shadow cone, in the shape of a paraboloid formed behind the target atom as shown in Fig. 2. Ion trajectories do not penetrate into the shadow cone, but instead are concentrated at its edges much like rain pours off an umbrella. Atoms located inside the cone behind the target atom are shielded from the impinging ions as shown in Fig. 3. Similarly, if the scattered ion or recoiling atom trajectory is directed towards a neighboring atom, that trajectory will be blocked. For a large number of scattering or recoiling trajectories, a blocking cone will be formed behind the neighboring atom into which no particles can penetrate. The dimensions of the shadowing and blocking cones can be determined experimentally from scattering measurements along crystal azimuths for which the interatomic spacings are accurately known. This provides an experimental determination of the scaling parameter C and reliable cone dimensions. The cone dimensions can also be constructed theoretically from the relationship of p with θ and ϕ [36,37]. A universal shadow cone curve has been proposed [38] and cone dimensions for common ion–atom combinations have been reported [39]. Since the radii of these cones are of the same order as interatomic spacings, that is 1 to 2 Å, the ions penetrate only into the outermost surface layers.

2.4. Scattering and recoiling anisotropy caused by shadowing and blocking cones

When an isotropic ion fluence impinges on a crystal surface at a specific incident angle α, the scattered and recoiled atom flux is anisotropic. This anisotropy is a result of the incoming ion's eye view of the surface, which depends on the specific arrangement of atoms and the shadowing and blocking cones. The arrangement of atoms controls the atomic density along the azimuths and the ability of ions to channel, that is, to penetrate into empty spaces between atomic rows. The cones determine which nuclei are screened from the impinging ion flux and which exit trajectories are blocked as depicted in Fig. 3. By measuring the ion and atom flux at specific scattering and recoiling angles as a function of ion beam incident α and azimuthal δ angles to the surface, structures are observed which can be interpreted in terms of the interatomic spacings and shadow cones from the ion's eye view.

2.5. Ion–surface electronic transitions

Electron exchange [40] between ions or atoms and surfaces can occur in two regions, (i) along the incoming and outgoing trajectories where the particle is within ångströms of the surface and (ii) in the close atomic encounter where the core electron orbitals of the collision partners overlap. In region (i), the dominating processes are resonant and Auger electron tunneling transitions,

both of which are fast ($\tau < 10^{-15}$ s). Since the work functions of most solids are lower than the ionization potentials of most gaseous atoms, keV scattered and recoiled species are predominately neutrals as a result of electron capture from the solid. In region (ii), as the interatomic distance R decreases, the atomic orbitals (AOs) of the separate atoms of atomic number Z_1 and Z_2 evolve into molecular orbitals (MOs) of a quasi-molecule and finally into the AO of the "united" atom of atomic number $(Z_1 + Z_2)$. As R decreases, a critical distance is reached where electrons are promoted into higher energy MOs because of electronic repulsion and the Pauli exclusion principle. This can result in collisional reionization of neutral species. The fraction of species scattered and recoiled as ions is sensitive to atomic structure through changes in electron density along the trajectories.

3. Instrumentation

The basic requirements [13] for low energy ion scattering are an ion source, a sample mounted on a precision manipulator, an energy or velocity analyzer, and a detector. The sample is housed in an ultra-high vacuum (UHV) chamber in order to prepare and maintain well-defined clean surfaces. The UHV prerequisit necessitates the use of differentially pumped ion sources. Ion scattering is typically done in a UHV chamber which houses other surface analysis techniques such as low energy electron diffraction (LEED), X-ray photoelectron spectroscopy (XPS), and Auger electron spectroscopy (AES). The design of an instrument for ion scattering is based on the type of analyzer to be used. An electrostatic analyzer (ESA) measures the kinetic energies of ions while a time-of-flight (TOF) analyzer measures the velocities of both ions and neutrals.

Ion source and beam line – The critical requirements for the ion source are that the ions have a small energy spread, there are no fast neutrals in the beam, and the available energy is 1–5 keV. Both noble gas and alkali ion sources are common. For TOF experiments, it is necessary to pulse the ion beam by deflecting it past an aperature. A beam line for such experiments is shown

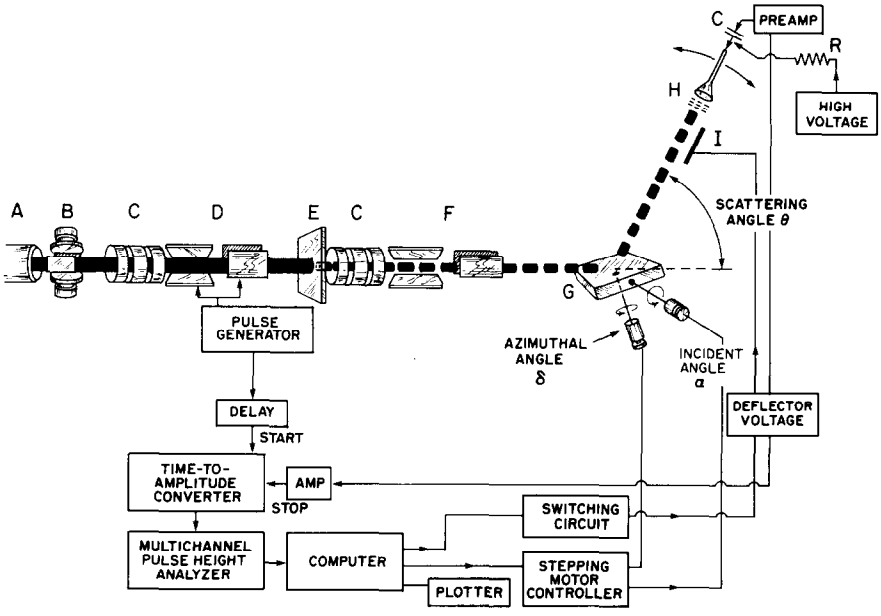

Fig. 4. Schematic drawing of TOF-SARS Spectrometer system. A = ion gun, B = Wien filter, C = Einzel lens, D = pulsing plates, E = pulsing aperture, F = deflector plates, G = sample, H = electron multiplier detector with energy prefilter grid and I = electrostatic deflector.

in Fig. 4; it is capable of producing ion pulse widths of ~ 15 ns.

Analyzers – An ESA provides energy analysis of the ions with high resolution. A TOF analyzer provides velocity analysis of both fast neutrals and ions with moderate resolution. In an ESA the energy separation is made by spatial dispersion of the charged particle trajectories in a known electrical field. ESA's were the first analyzers used for ISS; their advantage is high energy resolution and their disadvantages are that they analyze only ions and have poor collection efficiency due to the necessity for scanning the analyzer. A TOF analyzer is simply a long field-free drift region. It has the advantage of high efficiency since it collects both ions and fast neutrals simultaneously in a multichannel mode; its disadvantage is only moderate resolution.

Detectors – The most common detectors used for ISS are continuous dynode channel electron multipliers or channel plates which are capable of multiplying the signal pulses by 10^6–10^7. They are sensitive to both ions and fast neutrals. Neutrals with velocities $\gtrsim 10^6$ cm/s are detected with the same efficiency as ions.

4. Elemental analysis from scattering and recoiling

4.1. Qualitative analysis

TOF-SARS is capable of detecting all elements by either scattering, recoiling, or both techniques. TOF peak identification is straightforward by converting Eqs. (1) and (2) to the flight times of the scattered t_S and recoiled t_R particles as

$$t_S = L(M_1 + M_2)/(2M_1E_0)^{1/2} \times \left\{\cos\theta + \left[(M_2/M_1)^2 - \sin^2\theta\right]^{1/2}\right\} \quad (4)$$

and

$$t_R = L(M_1 + M_2)/(8M_1E_0)^{1/2}\cos\phi, \quad (5)$$

where L is the flight distance, that is, the distance from target to detector. Collection of neutrals plus ions results in scattering and recoiling

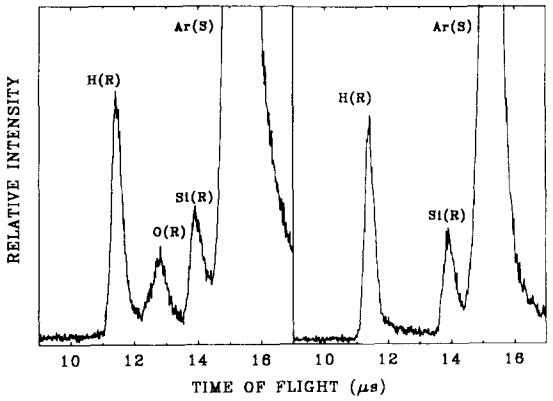

Fig. 5. TOF spectra of a Si(100) surface with chemisorbed H_2O (left) and H_2 (right). Peaks due to scattered Ar and recoiled H, O, and Si are observed. Conditions: 4 keV Ar^+, scattering angle $\theta = 28°$, incident angle $\alpha = 8°$.

intensities that are determined by elemental concentrations, shadowing and blocking effects, and classical cross sections. The main advantage of TOF-SARS for surface compositional analyses is its extreme surface sensitivity as compared to the other surface spectrometries, i.e. mainly XPS and AES. Indeed with a correct orientation and aperture of the shadow cone, the first monolayer can be probed selectively. At selected incident angles, it is possible to delineate signals from specific subsurface layers. Detection of the particles independently of their charge state eliminates ion neutralization effects. Also, the multichannel detection requires primary ion doses of only ~ 10^{11} ions/cm^2 or ~ 10^{-4} ions/surface atom for spectral acquisition; this ensures true static conditions during analyses.

TOF spectra – Examples of typical TOF spectra obtained from 4 keV Ar^+ impinging on a Si{100} surface with chemisorbed H_2O and H_2 are shown in Fig. 5 [41]. Peaks due to Ar scattering from Si and recoiled H, O, and Si are observed. The intensities necessary for structural analysis are obtained by integrating the areas of fixed time windows under these peaks.

4.2. Quantitative analysis

While qualitative identification of scattering and recoiling peaks is straightforward, quantita-

tive analysis requires relating the scattered or recoiled flux to the surface atom concentration. The flux of scattered or recoiled atoms F depends upon the primary ion flux F_p and the experimental geometry $f(\theta, \phi)$ as well as the following three factors: (1) the concentration of surface atoms C; (2) the degree to which shadowing and blocking attenuates the scattered and recoiled particles, as represented by a masking factor $a(E_0, E_S, E_R, \theta, \phi))$ with range $0 \leq a \leq 1$; and (3) the differential scattering or recoil cross section $\sigma(E_0, E_S, E_R, \theta, \phi)$. This can be expressed as

$$F = F_p f C \sigma (1 - a). \tag{6}$$

Compositional analyses by TOF-SARS and ISS have been applied in different areas of surface science, mainly in situations where the knowledge of the uppermost surface composition (first monolayer) is crucial. Some of these areas are as follows: gas adsorption, surface segregation, compounds and polymer blends, surface composition of real supported catalysts, surface modifications due to preferential sputtering by ion beams, diffusion, thin film growth and adhesion.

5. Structural analysis from TOF-SARS

The atomic structure of a surface is usually not a simple termination of the bulk structure. A classification exists based on the relation of surface to bulk structure. A *bulk truncated* surface has a structure identical to that of the bulk. A *relaxed* surface has the symmetry of the bulk structure but different interatomic spacings. With respect to the first and second layers, *lateral relaxation* refers to shifts in layer registry and *vertical relaxation* refers to shifts in layer spacings. A *reconstructed* surface has a symmetry different from that of the bulk symmetry. The

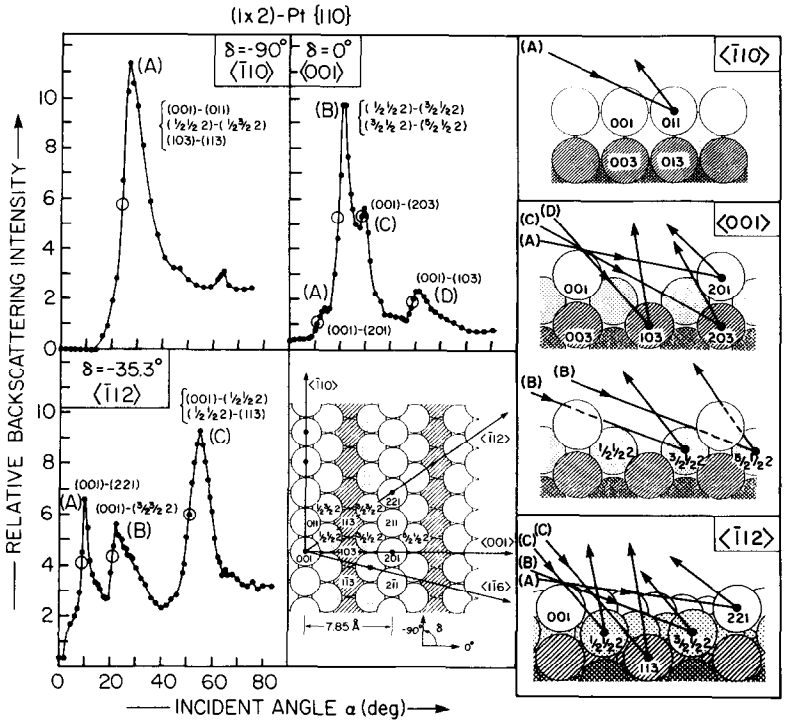

Fig. 6. Scattering intensity versus incident angle α scans for (1 × 2)-Pt{110} at $\theta = 149°$ along the ⟨1̄10⟩, ⟨001⟩ and ⟨1̄12⟩ azimuths. A top view of the (1 × 2) missing-row Pt{110} surface along with atomic labels is shown. Cross-section diagrams along the three azimuths illustrating scattering trajectories for the peaks observed in the scans are shown on the right.

methods of structural analysis will be delineated below.

5.1. Scattering versus incident angle α scans

When an ion beam is incident on an atomically flat surface at grazing angles, each surface atom is shadowed by its neighboring atom such that only forwardscattering (FS) is possible; these are large impact parameter (p) collisions. As α increases, a critical value $\alpha^{i}_{c,sh}$ is reached each time the ith layer of target atoms moves out of the shadow cone allowing for large angle backscattering (BS) or small p collisions as shown in Fig. 3. If the BS intensity I(BS) is monitored as a function of α, steep rises [42] with well defined maxima are observed when the focused trajectories at the edge of the shadow cone pass close to the center of neighboring atoms (Fig. 6). From the shape of the shadow cone, i.e. the radius (r) as a function of distance (l) behind the target atom (Fig. 2), the interatomic spacing (d) can be directly determined from the I(BS) versus α plots. For example, by measuring $\alpha^{1}_{c,sh}$ along directions for which specific crystal azimuths are aligned with the projectile direction and using $d = r/\sin \alpha^{1}_{c,sh}$, one can determine interatomic spacings in the 1st atomic layer. The first/second-layer spacing can be obtained in a similar manner from $\alpha^{2}_{c,sh}$ measured along directions for which the first- and second-layer atoms are aligned, providing a measure of the vertical relaxation in the outermost layers.

5.2. Scattering versus azimuthal angle δ scans

Fixing the incident beam angle α and rotating the crystal about the surface normal while monitoring the backscattering intensity provides a scan of the crystal azimuthal angles δ [43]. Such scans reveal the periodicity of the crystal structure. For example, one can obtain the azimuthal alignment and symmetry of the outermost layer by using a low α value such that scattering occurs from only the 1st atomic layer. With higher α values, similar information can be obtained for the 2nd atomic layer. Shifts in the first/second-layer registry can be detected by carefully monitoring the $\alpha^{2}_{c,sh}$ values for 2nd-layer scattering along directions near those azimuths for which the 2nd-layer atoms are expected, from the bulk structure, to be directly aligned with the 1st-layer atoms. The $\alpha^{2}_{c,sh}$ values will be maximum for those δ values where the 1st- and 2nd-layer neighboring atoms are aligned.

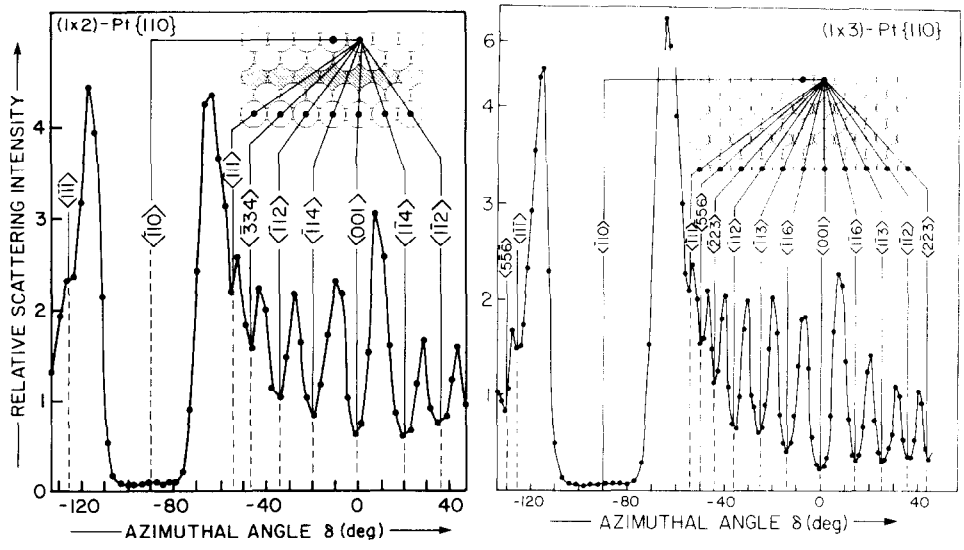

Fig. 7. Scattering intensity of 2 keV Ne^{+} versus azimuthal angle δ scans for Pt{110} in the (1 × 2) and (1 × 3) reconstructed phases. Scattering angle $\theta = 28°$ and incident angle $\alpha = 6°$.

When the scattering angle θ is decreased to a forward angle ($< 90°$), both shadowing effects along the incoming trajectory and blocking effects along the outgoing trajectory contribute to the patterns. The blocking effects arise because the exit angle $\beta = \theta - \alpha$ is small at high α values. Surface periodicity can be read directly from these features [39] as shown in Fig. 7 for Pt{110}. Minima are observed at the δ positions corresponding to alignment of the beam along specific azimuths. These minima are a result of shadowing and blocking along the close-packed directions, thus providing a direct reading of the surface periodicity.

Azimuthal scans obtained for three surface phases of Ni{110} are shown in Fig. 8 [44]. The minima observed for the clean and hydrogen-covered surfaces are due only to Ni atoms shadowing neighboring Ni atoms, whereas for the oxygen-covered surface minima are observed due to both O and Ni atoms shadowing neighboring Ni atoms. Shadowing by H atoms is not observed because the maximum deflection in the Ne^+ trajectories caused by H atoms is $< 2.8°$.

5.3. Recoiling versus incident angle α scans

Adsorbates can be efficiently detected by recoiling them into forward scattering angles ϕ as shown in Fig. 2. As α increases, the adsorbate atoms move out of their neighboring atom shadow cones so that direct collisions from incident ions are possible. When the p value necessary for recoiling of the adsorbate atom into a specific ϕ becomes possible, adsorbate recoils are observed with the TOF predicted from Eq. (5). Focusing at the edge of the shadow cone produces sharp rises in the recoiling intensity as a function of α. By measuring $\alpha_{c,sh}$ corresponding to the recoil event, we can directly determine the interatomic distance of the adsorbate atom relative to its nearest neighbors from p and the shape of the shadow cone.

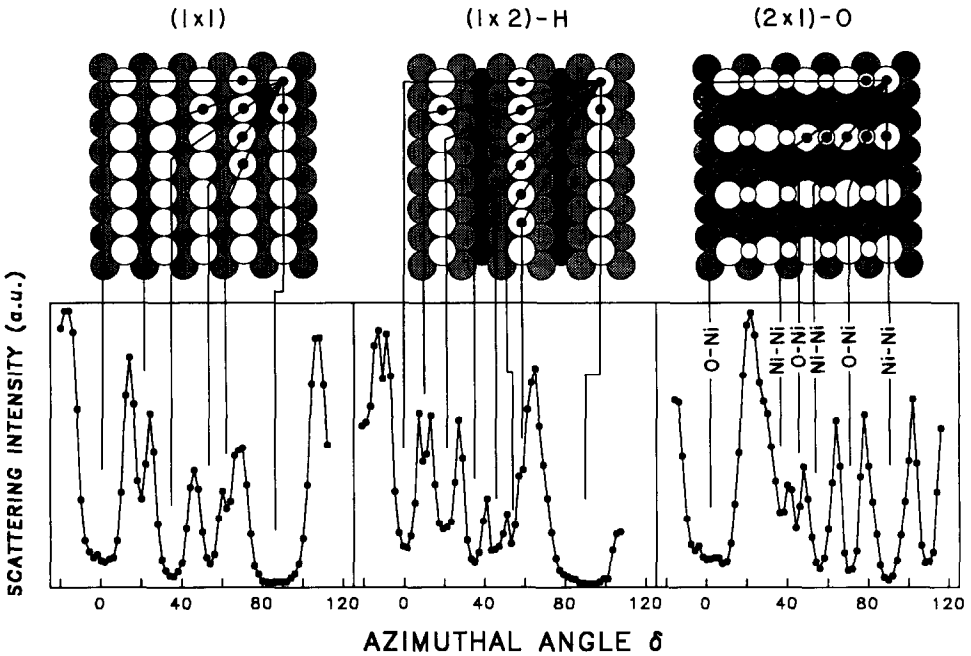

Fig. 8. Scattering intensity of 4 keV Ne^+ versus azimuthal angle δ for a Ni{110} surface in the clean (1 × 1), (1 × 2)-H missing row and (2 × 1)-O missing row phases. The hydrogen atoms are not shown. The oxygen atoms are shown as small open circles. O–Ni and Ni–Ni denote the directions along which O and Ni atoms, respectively, shadow the Ni scattering center.

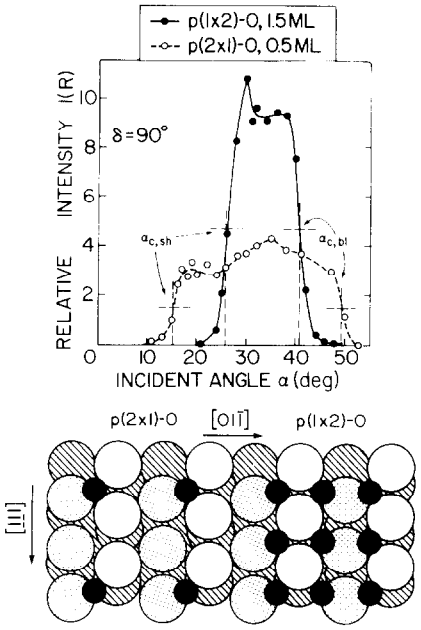

Fig. 9. Plots of oxygen recoil intensity versus incident angle α for both high (1.5 ML) and low (0.5 ML) oxygen coverages on a W{211} surface. The critical shadowing $\alpha_{c,sh}$ and blocking $\alpha_{c,bl}$ angle are indicated.

Example plots of oxygen recoil intensity versus α for two different chemisorbed O atom coverages on W{211} are shown in Fig. 9 [12]. Low dose exposure forms a p(2 × 1) structure consisting of 0.5 monolayer (ML) coverage and high dose exposure forms a p(1 × 2) structure consisting of 1.5 ML coverage. Sharp rises appear at low α and sharp decreases appear at high α. The rises are due to peaking of the ion flux at the edges of the shadow cones of neighboring atoms and the decreases are due to blocking of recoil trajectories by neighboring atoms. The critical α values for both shadowing, $\alpha_{c,sh}$, and blocking, $\alpha_{c,bl}$, can be used for determination of interatomic spacings. At high coverage, $\alpha_{c,sh} = 24°$ and $\alpha_{c,bl} = 42°$, which is considerably higher and lower, respectively, than the values $\alpha_{c,sh} = 16°$ and $\alpha_{c,bl} = 48°$ obtained at low coverage. This indicates that as coverage increases, both the shadowing and blocking effects are enhanced due to close packing of O atoms; this results from shadowing and blocking of O atoms by their neighboring O atoms. The α_c values correspond to O atoms

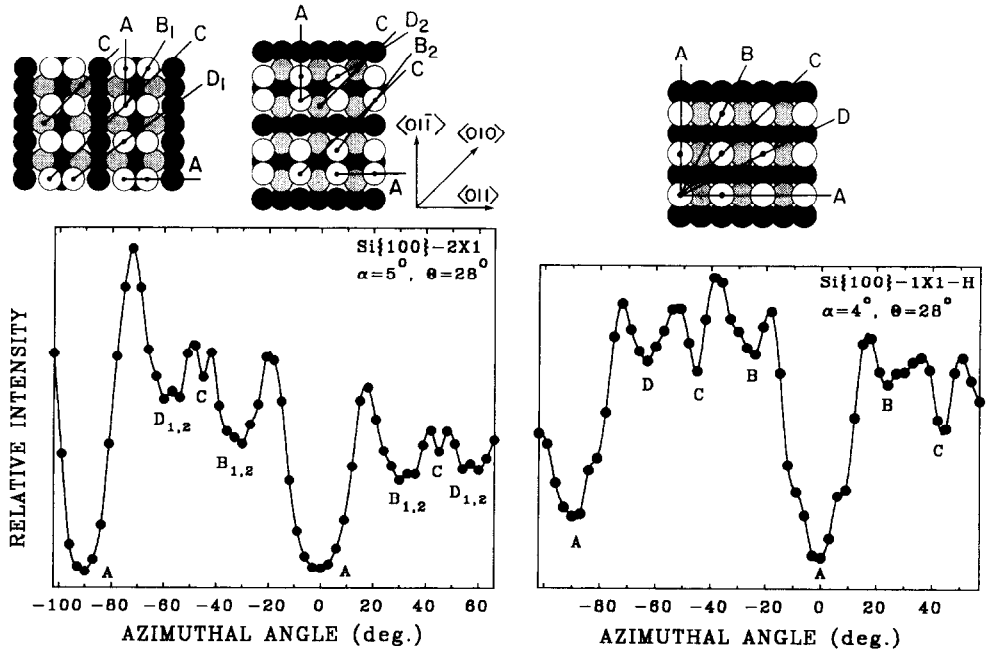

Fig. 10. Azimuthal angle δ scans of the silicon recoil intensity for the clean Si{100} and Si{100}-(1 × 1)-H dihydride surfaces. The minima are identified from the structural drawings above the scans. The hydrogen atoms are not shown.

separated by a distance of two W lattice constants at low coverage and one W lattice constant at high coverage.

5.4. Recoiling versus azimuthal angle δ scans

Plots of recoiling intensity versus azimuthal angle δ reveal the surface periodicity of the recoiled atoms in a manner similar to that of the scattering intensity. Azimuthal scans of Si recoils from the Si{100}-(2 × 1) and -(1 × 1)-H surfaces are shown in Fig. 10 [45]. The patterns are symmetrical about the ⟨011⟩ (δ = 0°) azimuth. The positions of the minima are consistent with the structures indicated above the figures. The repetition of the symmetry features every 90° indicates that there are two domains which are rotated by 90° with respect to each other. Azimuthal scans of H recoils from the Si{100}-(2 × 1)-H and Si{100}-(1 × 1)-H surfaces are shown in Fig. 11 [41]. The observed minima are due to Si atoms shadowing neighboring H atoms. The patterns are consistent with the structures indicated above the figures.

6. Ion–surface electron exchange from TOF-SARS

Ion–surface electron transition probabilities are determined by electron tunneling between the valence bands of the surface and the atomic orbitals of the ion. Such transition probabilities are highest for close distances of approach. Since TOF-SARS is capable of directly measuring the scattered and recoiled ion fractions, it provides an excellent method for studying ion–surface charge exchange. It has recently been shown that the charge transfer probabilities have a strong dependence on surface structure [46]. A direct method for measuring the spatial dependence of charge transfer probabilities with atomic-scale resolution has been developed using the method of direct recoil ion fractions [47]. The data demonstrate the need for an improved understanding of how atomic energy levels shift and broaden near surfaces. These types of measurements, combined with theoretical modeling, can provide a detailed microscopic map of the local reactivity of the surface. This information is of crucial importance for the understanding of vari-

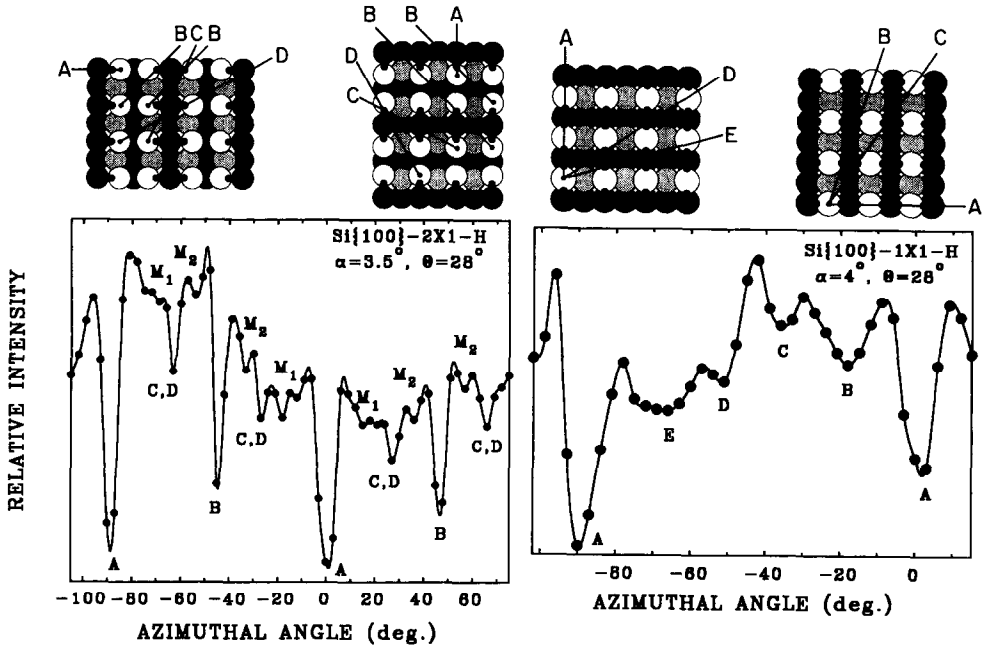

Fig. 11. Azimuthal angle δ scans of the hydrogen recoil intensity for a Si{100} surface in the (2 × 1)-H monohydride and (1 × 1)-H dihydride surfaces. The minima are identified from the structural drawings above the scans. The hydrogen atoms are indicated as small dark circles.

ous impurity-induced promotion and poisoning phenomena in catalysis and electron-density maps from scanning tunneling microscopy (STM).

7. Role of scattering and recoiling in the myriad of surface science techniques and expected new developments

Scattering and recoiling contribute to our knowledge of surface science through (i) elemental analysis, (ii) structural analysis, and (iii) analysis of electron exchange probabilities. We will consider the merits of each of these three areas.

7.1. Elemental analysis

The unique feature of scattering and recoiling spectrometry is the sensitivity to the outermost atomic layer of a surface. Using an ESA, it is possible to resolve ions scattered from all elements of mass greater than carbon. The TOF-SARS technique is sensitive to all elements, including hydrogen, although its limited resolution presents difficulties in resolving spectral peaks of high mass elements with similar masses. *The unique feature for elemental analysis is direct monitoring of surface hydrogen.* For general qualitative and quantitative surface elemental analyses, XPS and AES remain the techniques of choice.

7.2. Structural analysis

The major role of TOF-SARS is as a surface structure analysis technique which is capable of probing the positions of all elements with an accuracy of $\lesssim 0.1$ Å. TOF-SARS is sensitive to short-range order, i.e., individual interatomic spacings along azimuths. It provides a direct measure of interatomic distances in the first and subsurface layers and a measure of surface periodicity in real space. *One of its most important applications is the direct determination of hydrogen adsorption sites by recoiling spectrometry* [12,41]. Most other structure techniques fail for H atom determinations, with the possible exception of He atom scattering, VLEED, and vibrational spectroscopy

TOF-SARS is complementary to low energy electron diffraction (LEED), which probes long-range order, minimum domain size of 100 to 200 Å, and provides a measure of surface and adsorbate symmetry in reciprocal space. Coupling TOF-SARS and LEED provides a powerful combination for surface structure investigations. The techniques of medium and high (Rutherford backscattering) energy ion scattering sample subsurface and bulk structure and are not as surface sensitive as TOF-SARS.

New developments in structural applications of ion scattering are occurring rapidly. Coaxial ion scattering, in which the ion beam goes through a hole in a channel plate detector, allowing detection of $\sim 180°$ backscattered particles has been demonstrated [48,49]. Since this apparatus fits on a single flange, it is suitable for in situ monitoring of epitaxial film growth of atomic layers and for time-resolved analysis of dynamical surface processes. Improvements in optics will provide narrower ion pulse widths, resulting in enhanced time resolution of the spectra. Fast programs for computer simulation of scattering and recoiling trajectories have recently been developed [50]. These are extremely valuable in solving unknown structures by comparison of experimental data to simulations based on proposed structural models. Development of the simulations will make computer modeling of surface structures routine.

Future designs of scattering and recoiling instruments using large area detectors with position and time resolution of the events and fast electronics will be able to collect surface structural images on a very short time scale, allowing one to monitor dynamic processes at surfaces in real time. This will make it possible to monitor the dynamics of film deposition, chemisorption, surface reconstruction, surface diffusion, etc.

7.3. Ion–surface electron exchange probabilities

One of the unsolved problems in the interaction of low energy ions with surfaces is the mechanism of charge transfer and prediction of the charge composition of the flux of scattered, recoiled, and sputtered atoms. The ability to collect spectra of neutrals plus ions and only neutrals

provides a direct measure of scattered and recoiled ion fractions. Plots of ion fractions in incident- and azimuthal-angle space provide electronic transition probability contour maps which are related to surface electron density and reactivity along the various azimuths [47]. The application of TOF-SARS techniques to ion–surface electron exchange processes can develop into *a method* [47] *for determining local electron tunneling rates within the surface unit cell.*

8. Conclusions

Emphasis in this article has been placed on the physical concepts and structural applications of TOF-SARS. TOF-SARS is now well established as a surface structural analysis technique that will have a significant impact in areas as diverse as thin film growth, catalysis, hydrogen embrittlement and penetration of materials, surface reaction dynamics, and analysis of interfaces. Surface crystallography is evolving from the classical concept of a static surface and the question of "where do atoms sit?" to the concept of a dynamically changing surface. The development of large area detectors with rapid acquisition of scattering and recoiling structural images, as described in Section 7, will provide a technique for capturing time-resolved snapshots of such dynamically changing surfaces.

Acknowledgements

This material is based on work supported by the National Science Foundation under grant no. CHE-8814337, the R.A. Welch Foundation under grant no. E-656, and the Texas Advanced Research Program under grant no. 3652022ARP.

References

[1] D.P. Smith, J. Appl. Phys. 38 (1967) 340.
[2] W. Heiland and E. Taglauer, Surf. Sci. 68 (1977) 96; 47 (1975) 234; Radiat. Eff. 19 (1973) 1;
W. Heiland, F. Iberl, E. Taglauer and D. Menzel, Surf. Sci. 53 (1975) 383.
[3] H.H. Brongersma and J.B. Theeten, Surf. Sci. 54 (1976) 519;
H.H. Brongersma and P. Mul, Surf. Sci. 35 (1973) 393.
[4] E.P.Th.M. Suurmijer and A.L. Boers, Surf. Sci. 43 (1973) 309.
[5] A.G.J. DeWit, R.P.N. Bronckers and J.M. Fluit, Surf. Sci. 82 (1979) 177.
[6] M. Aono, Y. Hou, R. Souda, C. Oshima, S. Otani, Y. Ishizawa, K. Matsuda and R. Shimizu, Jpn. J. Appl. Phys. 21 (1982) L670;
M. Aono, Y. Hou, C. Oshima and Y. Ishizawa, Phys. Rev. Lett. 49 (1982) 567.
[7] M. Aono and R. Souda, Jpn. J. Appl. Phys. 24 (1985) 1249.
[8] H. Niehus, Surf. Sci. 145 (1984) 407;
H. Niehus and G. Comsa, Surf. Sci. 140 (1984) 18.
[9] L. Marchut, T.M. Buck, G.H. Wheatley and C.J. McMahon, Jr., Surf. Sci. 141 (1984) 549.
[10] J.M. van Zoest, J.M. Fluit, T.J. Vink and B.A. van Hassel, Surf. Sci. 182 (1987) 179.
[11] J.W. Rabalais, J.A. Schultz, R. Kumar and P.T. Murray, J. Chem. Phys. 78 (1983) 5250.
[12] J.W. Rabalais, O. Grizzi, M. Shi and H. Bu, Phys. Rev. Lett. 63 (1989) 51;
O. Grizzi, M. Shi, H. Bu, J.W. Rabalais, R.R. Rye and P. Nordlander, Phys. Rev. Lett. 63 (1989) 1408;
O. Grizzi, M. Shi, H. Bu and J.W. Rabalais, Phys. Rev. B 40 (1989) 10127;
H. Bu, O. Grizzi, M. Shi and J.W. Rabalais, Phys. Rev. B 40 (1989) 10147;
M. Shi, O. Grizzi, H. Bu, J.W. Rabalais, R.R. Rye and P. Nordlander, Phys. Rev. B 40 (1989) 10163.
[13] O. Grizzi, M. Shi, H. Bu and J.W. Rabalais, Rev. Sci. Instrum. 61 (1990) 740.
[14] J.W. Rabalais, Science 250 (1990) 521.
[15] M. Aono, M. Katayama and E. Nomura, Nucl. Instrum. Methods B 64 (1992) 29.
[16] A.H. Al-Bayati, K.G. Orrman-Rossiter, R. Badheka and D.G. Armour, Surf. Sci. 237 (1990) 213.
[17] R. Ghrayeb, M. Purushotham, M. Hou and E. Bauer, Phys. Rev. B 36 (1987) 7364.
[18] B.J.J. Koeleman, S.T. de Zwart, A.L. Boers, B. Poelsema and L.K. Verheij, Phys. Rev. Lett. 56 (1986) 1152.
[19] Th. Fauster, Vacuum 38 (1988) 129.
[20] M. Chester and T. Gustafsson, Surf. Sci. 256 (1991) 135.
[21] W. Hetterich, C. Höfner and W. Heiland, Surf. Sci. 251/252 (1991) 731.
[22] D.J. O'Connor, B.V. King, R.J. MacDonald, Y.G. Shen and X. Chen, Aust. J. Phys. 43 (1990) 601.
[23] A.I. Dodonoy, E.S. Mashkova and V.A. Molchanov, Radiat. Eff. Def. Solids 110 (1989) 227.
[24] M.H. Mintz, U. Atzmony and N. Shamir, Surf. Sci. 185 (1987) 413.
[25] E. van de Riet and A. Niehus, Surf. Sci. 243 (1991) 43.
[26] H. Niehus, R. Spitzl, K. Besocke and G. Comsa, Phys. Rev. B 43 (1991) 12619.
[27] F. Shoji, K. Kashihara, K. Sumitomo and K. Oura, Surf. Sci. 242 (1991) 422.

[28] S.H. Overbury, D.R. Mullins, M.T. Paffett and B.E. Koel, Surf. Sci. 254 (1991) 45.
[29] E. Taglauer, M. Beckschulte, R. Margraf and D. Mehl, Nucl. Instrum. Methods B 35 (1988) 404.
[30] D.M. Cornelison, M.S. Worthington and I.S.T. Tsong, Phys. Rev. B 46 (1990) 4051.
[31] J. Vrijmoeth, A.G. Schins and J.F. van der Veen, Phys. Rev. B 40 (1989) 3121.
[32] J.H. Huang and R.S. Williams, Phys. Rev. B 38 (1988) 4022.
[33] M.J. Ashwin and D.P. Woodruff, Surf. Sci. 237 (1990) 108.
[34] E.G. Mcrae, T.M. Buck, R.A. Malic, W.E. Wallace and J.M. Sanchez, Surf. Sci. Lett. 238 (1990) L481.
[35] G. Bracco, M. Canepa, P. Catini, F. Fossa, L. Mattera, S. Terreni and D. Truffelli, Surf. Sci. 269/270 (1992) 61.
[36] E.S. Mashkova and V.A. Molchanov, Medium-Energy Ion Reflection From Solids (North-Holland, Amsterdam, 1985).
[37] J.F. Zeigler, J.P. Biersack and U. Littmark, The Stopping and Range of Ions in Solids (Pergamon, New York, 1985).
[38] O.S. Oen, Surf. Sci. 131 (1983) L407.
[39] C.S. Chang, U. Knipping and I.S.T. Tsong, Nucl. Instrum. Methods B 18 (1986) 11; B 35 (1988) 151.
[40] S.R. Kasi, H. Kang, C.S. Sass and J.W. Rabalais, Surf. Sci. Rep. 10 (1989) 1.
[41] M. Shi, Y. Wang and J.W. Rabalais, Phys. Rev. B 48 (1993) 1689.
[42] F. Masson and J.W. Rabalais, Surf. Sci. 253 (1991) 245; 258.
[43] F. Masson and J.W. Rabalais, Chem. Phys. Lett. 179 (1991) 63.
[44] C.D. Roux, H. Bu and J.W. Rabalais, Surf. Sci. 259 (1991) 253;
H. Bu, C.D. Roux and J. W. Rabalais, Surf. Sci. 271 (1992) 68.
[45] Y. Wang, M. Shi and J.W. Rabalais, Phys. Rev. B 48 (1993) 1678.
[46] C.C. Hsu and J.W. Rabalais, Surf. Sci. 256 (1991) 77.
[47] C.C. Hsu, H. Bu, A. Bousetta, J.W. Rabalais and P. Nordlander, Phys. Rev. Lett. 69 (1992) 188; Phys. Rev. B 47 (1993) 2369.
[48] Y. Wang, M. Shi and J.W. Rabalais, Nucl. Instrum. Methods B 62 (1992) 505.
[49] M. Aono, M. Katayama and E. Nomura, Nucl. Instrum. Methods B 64 (1992) 29.
[50] R.S. Williams, M. Kato, R.S. Daly and M. Aono, Surf. Sci. 225 (1990) 355;
S. Chaudhury and R.S. Williams, Surf. Sci. 255 (1991) 127.